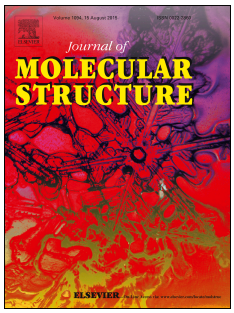

Synthesis, molecular structure, spectroscopic and theoretical investigation of 5-chlorosalicylaldehyde-2,4-dinitrophenylhydrazone

Diego M. Gil

PII: S0022-2860(19)31698-9

DOI: https://doi.org/10.1016/j.molstruc.2019.127589

Reference: MOLSTR 127589

To appear in: *Journal of Molecular Structure*

Received Date: 10 October 2019

Revised Date: 12 December 2019

Accepted Date: 13 December 2019

Please cite this article as: D.M. Gil, Synthesis, molecular structure, spectroscopic and theoretical investigation of 5-chlorosalicylaldehyde-2,4-dinitrophenylhydrazone, *Journal of Molecular Structure* (2020), doi: https://doi.org/10.1016/j.molstruc.2019.127589.

Graphical abstract

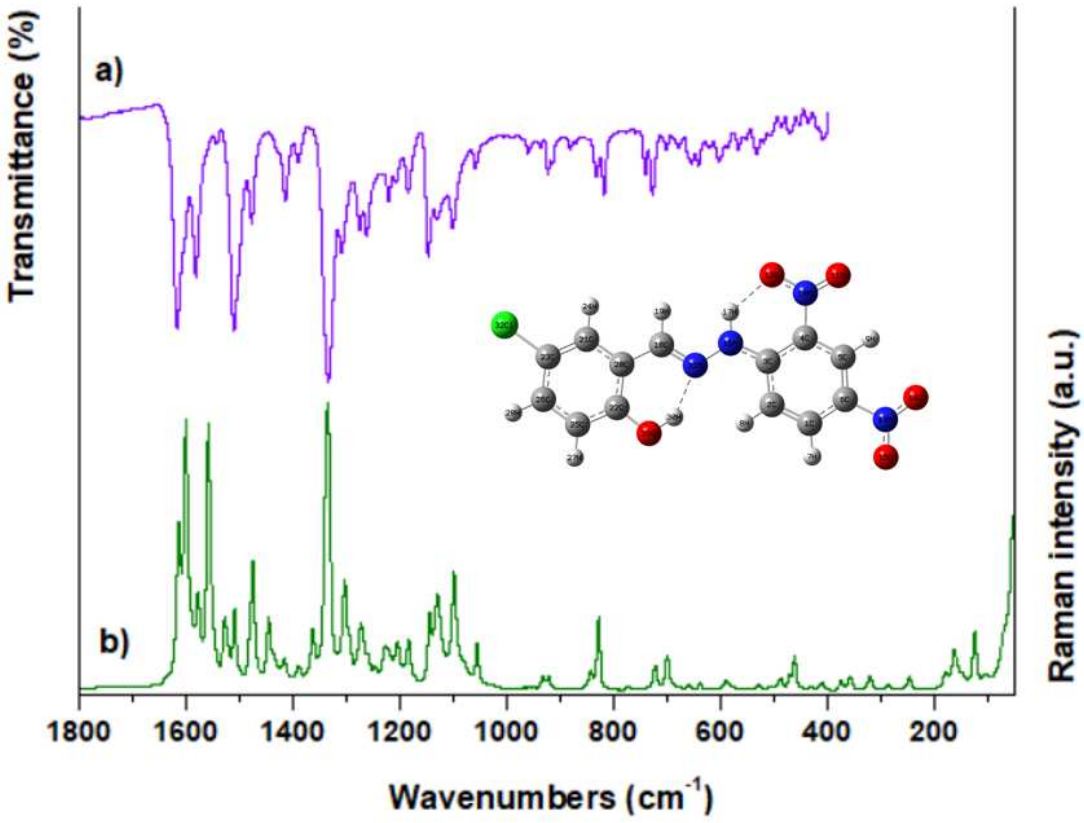

Synthesis, molecular structure, spectroscopic and theoretical investigation of 5-chlorosalicylaldehyde-2,4-dinitrophenylhydrazone.

Diego M. Gil[1,+,*]

[1] INBIOFAL (CONICET-UNT). Instituto de Química Orgánica. Facultad de Bioquímica, Química y Farmacia. Universidad Nacional de Tucumán. Ayacucho 471. T4000INI. San Miguel de Tucumán. Argentina.

[+] Member of the Research Career of CONICET.

[*] Corresponding author: dmgil@fbqf.unt.edu.ar (Dr. Diego M. Gil)

Abstract

A new hydrazone derivative, 5-chlorosalicylaldehyde-2,4-dinitrophenylhydrazone (5Cl-DNPHZ) has been synthesized and characterized by different spectroscopic techniques such as IR, Raman and UV-Vis. A combined experimental and quantum chemical approach was performed to study the structural and spectroscopic properties of the title compound. The effect of substituents (chlorine and hydroxyl) on the benzene ring on the structural and electronic properties of 5Cl-DNPHZ and a related compound DNPHZ previously reported are analysed. Natural bond orbital (NBO) analysis was performed to obtain information about the interactions that were responsible for the stability of the different conformers of the title compound. The Atoms in molecules (AIM) calculations revealed that the intramolecular hydrogen bonding interactions observed in both conformations are of *core-shell* in nature. The molecular electrostatic potential (MEP) surface of the most stable conformer of 5Cl-DNPHZ shows that the oxygens of the nitro groups are prone to electrophilic attack and the hydrogen of the hydrazine group is prone to nucleophilic attack indicating that the intramolecular hydrogen bonding interaction is favoured between both groups.

Keywords: Hydrazone derivative, DFT calculations, AIM approach, Vibrational study

1. INTRODUCTION

Hydrazone compounds, with general formula RR'C=N-NHR'' (R= alkyl or aryl groups), are good candidates for the development of new drugs. These compounds are generally obtained by heating the appropriate substituted hydrazine or hydrazide with a ketones or aldehydes in different solvents such as ethanol, methanol, THF, buthanol or glacial acetic acid. Hydrazones can be used as intermediates in the synthesis of hydrazine derivatives by reduction of hydrazine with $NaBH_4$ **[1]** or heterocycle compounds such as 1,3,4-oxadiazolines, 2-azetidinones, thiazolidinones, triazolines and pyrazoles **[2-4]**. The chemical versatility of hydrazones is mainly attributed to the functional diversity of the imine functional group (C=N-N-) which has nitrogens with nucleophilic character, an imine carbon with both electrophilic and nucleophilic character and configurational isomerism around the C=N double bond. These structural features of the imine group are mainly responsible of the physical and chemical properties of hydrazones derivatives. They are found to have versatile coordinating abilities towards different metal ions leading stable coordination compounds **[5-9].** Numerous hydrazone compounds exhibit efficient non-linear optical (NLO) properties due to their potentially high nonlinear optical effects and rapid response in electro-optic devices, optical modulation, molecular switching, optical memory and frequency doubling **[10, 11]**. In particular, hydrazones derived from *o*-hydroxyaromatic aldehydes and ketones show two prototropic tautomeric forms, the keto and phenol hydrazine forms. This tautomerism arise from intramolecular transfer process in which the H atom from the hydroxyl group is transferred to the imine N atom. The appearance of these tautomeric forms separately or jointly depends on the media and substituents that provide different electron-donating or withdrawing systems **[12]**. Shang and co-workers have reported the tautomeric equilibria between keto and phenol-hydrazone forms induced by different anions in solution and the tautomeric equilibria occurred during the anion recognition process **[13]**.

It is well-known that hydrazones exhibit diverse biological and pharmacological activity in medicinal chemistry as were reviewed recently **[14, 15]**. In general, hydrazones have been reported as anti-microbial, anti-bacterial, anti-fungal, anti-viral, anti-malarial, anti-tumor, anti-cancer, anti-convulsant, analgesic and anti-inflammatory agents **[14, 15]**. Furthermore, hydrazones generally exhibit physiological properties in the treatment of some diseases such as tuberculosis, due to the formation of metal complexes with metals which catalyse physiological processes **[16]**.

2,4-dinitrophenylhydrazine (2,4-DNPH) is a nitro-substituted phenylhydrazine with an intense reddish colour and it was used in the analysis of aldehydes and ketones (both for characterizing the carbonyl functional group and identifying such compounds by the melting points of their derivatives). Hydrazones involving 2,4-DNPH have received special attention because of their interesting biological properties and the formation of transition metal complexes **[17-19]**. Structural properties of salicylhydrazones derived from 2,4-DNPH have been studied in solid state indicating that only the hydrazine tautomeric form is present in the crystalline state stabilized by O-H···N and N-H···O(nitro) intramolecular interactions **[20-22]**.

In view of the mentioned properties and applications of hydrazones, the 5-chlorosalicylaldehyde-2,4-dinitrophenylhydrazone, and it will be referred as 5Cl-DNPHZ (see *Scheme 1*) has been synthesized and characterized by different spectroscopic techniques such as IR, Raman and UV-Visible spectra. The experimental results were complemented with quantum chemical calculations by using DFT methods. Natural Bond Orbital (NBO) and atoms in molecules (AIM) analysis have been performed to evaluate the strength and stability of the intramolecular hydrogen bonding interactions. The molecular electrostatic potential (MEP) were calculated in order to know structure-reactivity relationships and reactive sites of the title compound. In addition, I have investigated the effect of the inclusion of a chlorine atom in the structure of the aromatic ring on the electronic properties and reactivity in gas phase and in different solvents. Also, I have performed a comparison between the title molecule (5Cl-DNPHZ) and a related Schiff base N-(2,4-Dinitrophenyl)-N'-(1-phenylethylidene)-hydrazine (DNPHZ) previously reported **[20] (**see *Scheme 1***)**.

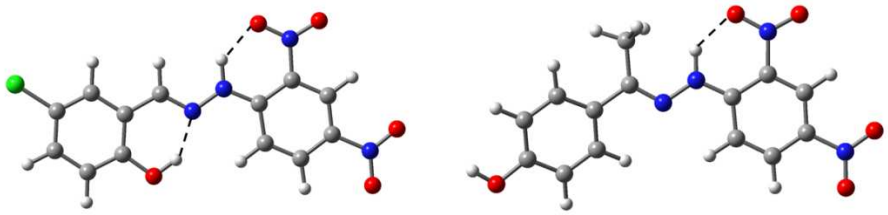

5Cl-DNPHZ ***DNPHZ***

Scheme 1. *Schematic representation of the hydrazone obtained from 5-chlorosalicylaldehyde and 2,4-DNPH (5Cl-DNPHZ) and a related molecule (DNPHZ).*

2. EXPERIMENTAL DETAILS

2.1. Synthesis

All chemicals were of analytical grade and were used without further purification. The title compound was synthesized by reflux of ethanolic solutions of 2,4-DNPH (1 mmol) and 5-chlorosalycylaldehyde (1 mmol) in presence of 3 drops of glacial acetic acid. After refluxing for 30 minutes, a reddish precipitate appeared and the mixture was refluxed for 3 hours. The solid was separated from the solution by filtration and washed with cold ethanol. Yield: 80 %. Melting point: 275-278 ºC. (336.5) Anal. Calcd for $C_{13}H_9O_5N_4Cl$ (%): C: 46.36, H: 2.67, N: 16.64; Found (%): C: 46.41, H: 2.72, N: 16.75.

2.2. Instrumentation

Carbon, hydrogen and nitrogen elemental analysis were measured on a Carlo Erba analyzer. The solid state IR spectra were recorded at room temperature on a FTIR Perkin Elmer GX1 in the frequency range 4000-400 cm^{-1} using KBr pellets (4 cm^{-1} of spectral resolution). The Raman dispersion spectra were measured on a Thermoscientific DXR Raman microscope, in the 3500-50 cm^{-1} range using a diode-pump solid state laser of 532 nm, with a spectral resolution of 5 cm^{-1}. The electronic absorption spectra of the title compound ($5 \cdot 10^{-5}$ M) was measured on DMF solution, in the 200-800 nm spectral range using a quartz cell with 10 mm of optical path length.

2.3. Computational methods

All quantum chemical calculations were performed with Gaussian 03 program package **[23]**. Becke's three parameter hybrid model along with Lee-Yang-Parr correlation functional (B3LYP) method and 6-311++G(d,p) basis sets was used for all calculations including geometry optimization and vibrational frequency. The calculated vibrational frequencies corresponded in all cases to potential energy minima for which no imaginary frequencies were found. Natural Bond Orbital (NBO) analysis were performed for 5Cl-DNPHZ and DNPHZ at B3LYP/6-311++G(d,p) approximation and the energy of the donor-acceptor interactions were estimated by the second-order perturbation theory **[24]**. The electron density analysis was accomplished by using the Atoms in Molecules theory **[25]** implemented in the AIM2000 code **[26]**. The absorption spectra of the title compound in gas phase and taken into account the implicitly of the solvent (DMF) were calculated with the time-dependent density functional theory (TD-DFT) method **[27]**. In addition, the electronic properties such as

HOMO and LUMO energies were determined in gas phase and in different solvents such as toluene, chloroform, ethanol and dimethylformamide. By using HOMO-LUMO analysis, various global reactivity descriptors such as chemical hardness, chemical potential, softness, electrophilicity index and electronegativity were calculated for both molecules in gas phase and in the mentioned solvents.

3. RESULTS AND DISCUSSION

3.1. Conformational analysis and structural results

The potential energy curves for the internal rotation of the C18-C20 (**Figure 1**) were calculated at B3LYP/6-311++G(d,p) approximation to investigate the conformational stability of the title compound. The curve shows two minima, the first one located at 0º (conformer I) and the second at 180º (conformer II). As shown in **Figure 1**, the most stable conformer is stabilized mainly through intramolecular O29-H···N31 hydrogen bonding interactions between the hydrogen of the hydroxyl group and the N from the imine group. In addition, the planar conformation is also stabilized by intramolecular N16-H···O12 interactions involving the hydrazine N-H and the *ortho* nitro group. Theoretical calculations of the studied compound revealed also a local minimum for conformer II where the intramolecular O29-H···N31 interaction is absent. The relative energies of the conformers with respect to the most stable conformer CI are shown in **Table S1** (Supplementary Information). The large differences in total energy (ΔE_{CII-CI} = 7.57 kcal/mol) and in free energy (ΔG_{CII-CI} = 7.31 kcal/mol) indicate that only the conformer I could be observed in solid phase. The geometry of the related compound DNPHZ is also planar, with C-N-N-C dihedral angle of 173.2º. In this case, only the intramolecular N-H···O(nitro) hydrogen bonds are observed in the solid while the intramolecular O-H···N interactions are absent due to the location of the hydroxyl group (see *Scheme 1*) **[20]**. The optimized structural bond length, angles and torsional angles at B3LYP/6-311++G(d,p) approximation for CI and CII conformers are given in **Table 1** and they are compared with data reported for a related compound **[20]**. The molecular structures of both conformers are shown in **Figure 2** indicating that CI and CII conformers are structurally independent. Both conformers exists in *E*-configuration with respect to the 5-chlorosalicylaldehyde and 2,4-DNP groups located on the opposite side of the imine C18=N31 bond. In Conformer I for the title compound, the C18-N31 bond is longer than in Conformer II due to the presence of intramolecular O29-H30···N31 hydrogen bond. In this conformation, the C18=N31 and the H-O groups

form a pseudo 6-membered ring, with a distance N31···O29 of 2.684 Å which is considerably shorter than the sum of the van der Waals radii of N and O. For conformer I, the bond lengths C22-O29 and C18-N31 are 1.347 and 1.293 Å, respectively. These values are compatible with the properties of single and double bonds, which describes an *o*-hydroxy Schiff base in a phenol-imine tautomeric form. For both conformations, the bond angles C20-C18-N31 and C18-N31-N16 are consistent with the sp^2 hybrid character of C18 and N31 atoms (see Table 1). The N=O bonds of the nitro groups are asymmetrical, with bond lengths of 1.219 and 1.243 Å for N10=O11 and N10=O12 bonds, respectively for both conformers. These results are in agreement with the presence of intramolecular N16-H17···O12 hydrogen bonds (see Figure 2). It is well known that the nitro group is highly electronegative and electron withdrawing obtaining electron density from the benzene ring **[28]**. The two nitro groups located in the *ortho* and *para* position in the benzene ring produce an elongation of the C3-C4 (1.429 Å) and C2-C3 (1.418 Å) as compared to C4-C5 (1.393 Å) and C6-C1 (1.400 Å) bonds. The C-N bond length of the attached nitro groups are calculated to be 1.460 and 1.468 Å, in agreement with reported values in literature **[20]**. The N16-C3 bond lengths are predicted to be 1.360 and 1.362 Å for conformers I and II, respectively. These values are lower than C-N single bond (1.47 Å) and longer than C=N double bonds (1.22 Å) indicating that the N16-C3 shows a partial double bond character. The theoretical values for N-N single bond are 1.360 and 1.356 Å for conformers I and II, respectively, in agreement with the reported value obtained from XRD data **[20]**. The distance C23-C26 in the title molecule is 1.397 Å, lower than the C-C distance reported for the molecule reported by Ning-Ning and co-workers for a related compound because the hydroxyl group attached to the C26 atom is probably involved in resonance with the aromatic ring leading a shortening in the C23-C26 bond distance **[20]**.

In accordance with the reported crystal structure of a related compound N-(2,4-Dinitrophenyl)-N'-(1-phenylethylidene)-hydrazine (DNPHZ) **[20]**, the crystal packing of the substance is stabilized by classical N-H···O(nitro) and non-classical C-H···O(nitro) intermolecular hydrogen bonds. Takinginto account these results, we have selected a dimer involving these intermolecular interactions. The optimized molecular structure of the dimer computed at B3LYP/6-311++G(d,p) approximation is shown in **Figure S1** (Supplementary Information). The proposed 5-Cl-DNPHZ dimer involves bifurcated hydrogen bonding interactions C21-H···O11 and C18-H···O11 between the O11 of the nitro group and the H atoms of the phenyl and imino groups, respectively.

The geometrical parameters for the hydrogen bonds calculated at B3LYP/6-311++G(d,p) level are shown in **Table S2** (Supplementary Information). In addition, classical N16-H···O12 hydrogen bonds are observed,with hydrogen bond distances of 2.479 Å.

3.2. Vibrational analysis

The experimental IR and Raman spectra of the title compound in solid state are shown in **Figure 3**. Observed and computed (unscaled and scaled) wavenumbers, together with a tentative assignment of modes for the most stable conformer (CI) are listed in **Table 2**. The vibrational spectra were assigned by comparison with the reported data for related compounds **[29-31]**, and on the basis of calculated wavenumbers at B3LYP/6-311++G(d,p) approximation and by using the potential energy distribution (PED) analysis. Comparison between experimental and calculated IR and Raman spectra of CI conformer of the title compound are shown in **Figures S2** and **S3** (Supplementary Information). The experimental wavenumbers are generally lower than computed ones due to the anharmonicity of molecular vibrations. For this reason, calculated wavenumbers were scaled using the scale factor 0.9679.

3.2.1. O-H and N-H vibrations. In the IR spectrum of the title compound in solid state, the band corresponding to the O-H stretching mode is observed at 3360 cm^{-1} as a broad band. The OH stretching vibration was calculated at 3496 cm^{-1} with the 99 % of PED contribution. The observed *ν*(OH) vibrational frequency and the broadening of this band in the IR spectrum of the solid is attributed to the intramolecular O-H···N hydrogen bonding interactions in solid state. The weak band observed at 1417 cm^{-1} in the IR spectra (1418 cm^{-1} in Raman) is assigned to the in-plane O-H bending mode while the out-of-plane O-H bending vibration mode appears as a weak band at 834 cm^{-1}, in accordance with related compounds **[32]**.

The N-H stretching vibration of the hydrazine group is observed as a weak band at 3287 cm^{-1} in the IR spectrum (3289 cm^{-1} in Raman). This frequency value is lower than that observed for similar compounds with the C=N-NH- moiety, usually at 3350 cm^{-1} **[33]**. Due to the nature of this vibration mode, its frequency value is very sensitive to the crystalline state, in which hydrogen bonding interactions of the type N-H···O are present and produce larger deviations between experimental and calculated values. In

addition, the red shift observed could be attributed to the intramolecular N-H···O hydrogen bond that affects the force constant of the hydrazine group.

3.2.2. C-H vibrations. The C-H stretching modes of substituted benzene derivatives are expected to appear in the region 3000-3125 cm^{-1} **[34]**. In the present study, the band at 3102 cm^{-1} in the IR spectra is assigned to C-H stretching mode of the benzene ring. In aromatic compounds, the C-H in-plane bending modes generally appear in the region 1400-850 cm^{-1} with low intensity while the C-H out-of-plane bending vibrations arises in the region 950-600 cm^{-1} with medium intensity **[35, 36].** The infrared bands at 1479, 1264, 1224, 1209 and 1103 cm^{-1}, with counterparts in Raman at 1476, 1447, 1263, 1228, 1206 and 1101 cm^{-1} are assigned to C-H in-plane bending modes. The out-of-plane C-H bending modes are also assigned and listed in Table 2. The theoretical values obtained at B3LYP/6-311++G(d,p) level are found to be in good agreement with the experimental observations.

3.2.3. C=N and N-N vibrations. The medium intensity band at 1582 cm^{-1} in the infrared spectrum, with a counterpart at 1580 cm^{-1} in Raman, is assigned to the C=N stretching vibration, with a 44 % contribution of PED. The presence of C=N stretching mode is an indicative of the presence of the hydrazine linkage in the title compound.

The υ(N-N) stretching vibration is clearly observed in the Raman spectrum at 1088 cm^{-1}, in good agreement with the computed value (1127 cm^{-1}).

3.2.4. C-O and C-C ring vibrations. The C-O stretching mode appears as a weak intensity band in the IR spectrum at 1278 cm^{-1} (1274 cm^{-1} in Raman). The computed value is consistent with the experimental value (36% PED).

The bands corresponding to the ring C-C stretching modes of the phenyl rings appear as medium to strong intensity absorptions in the fingerprint region. In the title compound, the bands at 1618, 1607, 1513, 1392, 1311, 1134 and 1060 cm^{-1} in the IR spectrum and the dispersion bands at 1615, 1603, 1560, 1529, 1511, 1391, 1364, 1305, 1186, 1133, 1088 and 1058 cm^{-1} in Raman are assigned to ring C-C stretching modes. The calculated values match well with the observed bands (see Table 2). The IR spectrum of the title compound shows absorption bands at 917, 834, 743, 664, 644 and 605 cm^{-1} (845, 661 and 640 cm^{-1} in Raman), which are assigned to the in-plane CCC bending

modes of the phenyl rings. The bands associated to out-of-plane and torsional modes of the phenyl rings are listed in Table 2.

3.2.5. NO_2 vibrations. The most characteristic bands in the IR spectra of nitro derivatives are attributed to antisymmetric and symmetric N=O stretching modes, which appear in the region 1550-1300 cm^{-1} **[37]**. The molecule studied in this work shows two nitro groups, one located at *ortho* and another at *para* position of the benzene ring. Generally, antisymmetric N=O stretching modes are always observed at higher wavenumbers than symmetric stretching vibration. The IR bands at 1543 and 1336 cm^{-1} are assigned to antisymmetric and symmetric N=O stretching modes, respectively. These modes appear at 1600 and 1349 cm^{-1} in the spectrum of free nitro groups **[38]**. The red-shift in the N=O stretching mode of the nitro groups located in the *ortho* position are due to the intramolecular hydrogen bonding interaction N-H···O(nitro), as was explained previously. The weak band at 821 cm^{-1} is assigned to in-plane bending mode of the NO_2 group whereas the bands at 704 and 681 cm^{-1} are attributed to out-of-plane NO_2 bending modes. These results are in agreement with the computed ones (see Table 2).

3.3. Electronic spectra

In order to understand various electronic transitions of the title compound, the electronic absorption spectrum for the singlet to singlet electronic transitions was computed for fully optimized ground state geometry. The electronic spectrum of the title molecule has been assigned with the help of calculations at B3LYP/6-311++G(d,p) level with PCM solvent modelling method in DMF as solvent. The experimental (measured in DMF) and calculated electronic absorption spectra of 5-Cl-DNPHZ are shown in **Figure 4**. The observed and calculated electronic transitions of high oscillator strengths and assignments are listed in **Table 3**. The absorption band at 463 nm in the calculated spectrum is assigned to HOMO → LUMO transition. This band was not clearly observed experimentally probably because it is obliterated by the much more intense absorption band at 506 nm, which correlates with the HOMO → LUMO+1 transition (calculated: 417 nm). The experimental maximum at about 478 nm corresponds to HOMO-1 → LUMO transition, in accordance with the calculated value at 349 nm. The band observed at 386 nm in the experimental spectrum of the title compound is attributable to HOMO-3 → LUMO transition, with 87 % of contribution.

Figure 5 shows selected frontier molecular orbitals involved in the main electronic transition of 5-Cl-DNPHZ with the corresponding energies. As shown in Figure 5, the HOMO involves π-bonding orbitals of the aromatic rings and the non-bonding character of the hydroxyl oxygen, chlorine atom and the N atom of the hydrazone bond. The LUMO exhibits a π anti-bonding character of carbon atoms and nitro groups of the 2,4-DNPH moiety. Thus, the HOMO → LUMO electronic transition has a π→π* nature.

3.4. Frontier molecular orbitals and global descriptors

The total energy, energy gap between HOMO and LUMO frontier molecular orbitals and dipole moment have an important effect in the stability of a molecule. Results obtained from calculations at B3LYP/6-311++G(d,p) level of theory in different solvents for 5Cl-DNPHZ and DNPHZ are listed in **Tables S3** and **S4** (Supplementary information).

The band gap between frontier molecular orbitals HOMO and LUMO is an important index which measures electron conductivity and determines chemical reactivity of a molecule. HOMO is associated with the ionization potential while LUMO is related to electron affinity of a molecule. With the HOMO-LUMO band gap, the electronegativity (χ), chemical potential (μ), chemical hardness (η), chemical softness (s) and electrophilicity index (ω) global descriptors were computed by using different equations reported in literature **[39]**. **Figures S4** and **S5** show the variation of dipole moment and $\Delta E_{HOMO-LUMO}$ with the dielectric constant of the solvents for 5Cl-DNPHZ and DNPHZ, respectively. In accordance with the results reported in **Tables S3** and **S4**, the HOMO-LUMO band gap is lower in magnitude for DNPHZ in all the solvents explaining the eventual charge transfer interactions taking place within the molecule. These results also indicate that DNPHZ is more reactive and less stable than 5Cl-DNPHZ. The calculations also indicate that the stability of both compounds decreases with the polarity of the solvent.

Dipole moment shows the molecular charge distribution and is given as a vector in three dimensions and it can be used as a descriptor to depict the charge movement across the molecule. The results listed in **Tables S3** and **S4** also indicates that DNPHZ is most stable than 5Cl-DNPHZ in all media due to the higher dipole moment values. Contrary to the $\Delta E_{HOMO-LUMO}$ energy gap, the dipole moment of both compounds increases with the polarity of the solvents (see **Fig. S4** and **S5**).

Comparing the global descriptors of both compounds, we observed that 5Cl-DNPHZ in all solvents shows higher electrophilicity indexes values than DNPHZ. The higher electrophilicity indexes observed for the most stable conformer of 5Cl-DNPHZ in all solvents could probably explain the potential biological activity for the mentioned compound. The chemical hardness is useful to rationalize the relative stability and reactive of different compounds. The values of chemical hardness are higher in all solvents for 5Cl-DNPHZ than DNPHZ. From **Tables S3** and **S4**, the chemical hardness increases in parallel with the increasing value of the HOMO-LUMO energy gap and the molecule becomes more stable. In addition, the chemical hardness decreases in parallel with the increasing of the polarity of the solvents.

3.5. NBO results and topological analysis

NBO analysis is an important method for the study the role of intra and intermolecular interactions, interactions among bonds and hyperconjugative and conjugative interactions in different molecular systems. These interactions can be quantitatively described in terms of NBOs stabilization energy (E^2) associated with delocalization of electron density from *i*(donor) to *j*(acceptor) as follow:

$$E^{(2)} = \Delta E_{ij} = q_i \frac{F_{ij}^2}{E_i - E_j} \qquad (1)$$

Where q_i is the donor orbital occupancy, E_i and E_j are the diagonal elements, and F_{ij} is the off-diagonal Fock matrix element. The large value of $E^{(2)}$ for a particular interaction indicates the greater delocalization of the electron density through these bonds. The results of second-order perturbation theory analysis calculated at B3LYP/6-311++G(d,p) level for conformers I and II are presented in **Table 4**. Interactions of π-electrons in the rings give the greatest intramolecular interactions energy for both conformations with $E^{(2)}$ values in the range 16.31-32.57 kcal/mol. Hyperconjugative σ → σ* interactions are weak and their energies are less than 5 kcal/mol. NBO analysis for both conformers of the title compound clearly indicates the presence of one lone pair orbital formally attached at the N16 atom. The nature of this orbital is a pure *p* type (LP_π N16), with a low electron occupancy of 1.61e indicating the electron-donating capacity for this orbital. In accordance with second-order perturbation approach, the lone pair orbital contributes to a strong resonance interactions with the phenyl ring, with an interaction energy LP N16 → π* C3-C4 of 54.82 and 54.44 kcal/mol for conformers I and II, respectively. This electron donation into the π* C3-C4 antibonding orbitals is

reflected also in its high electronic occupancy of 0.49e. In addition, the lone pair orbital of N16 donates electronic density mainly to the vacant C18-N31 antibonding orbital via a mesomeric interaction LP N16 → π* C18-N31 with $E^{(2)}$ values of 27.37 and 29.35 kcal/mol in conformers I and II, respectively. The most relevant donor-acceptor interactions have also been evaluated for both conformers (see Table 4). The LP O12 → π* N10-O11 interaction gives a strong stabilization to the system by 133.3 kcal/mol mainly due to charge transfer within the nitro group. The hyperconjugative interaction LP O12 → σ* N16-H7 are responsible for the intramolecular N16-H17···O12 that stabilizes the planar conformation of the title compound in both conformations. The chlorine substitution in the aromatic ring helps the conjugation of the entire system with LP Cl32 → π* C22-C25 interaction energies of 16.44 and 16.54 kcal/mol for conformers I and II, respectively. For the relative compound DNPHZ, the lone pair from the hydroxyl oxygen participates in LP O → π* C23-C26 interactions with an energy value of 28.84 kcal/mol, indicating that this interaction could produce a strong delocalization in the aromatic ring.

The total atomic charges for both conformation of the title compound are obtained from natural population analysis (NPA). These results revealed that the more negative charge (-0.69 a.u.) is located at the O29 atom of the hydroxyl group and the negative charges -0.44, -0.38 and -0.33 a.u. are located at the O12, N16 and N31, respectively. The more negative charge on O29 atom makes C22 atom more positive and acidic, with a charge of +0.37 a.u.

Atoms in Molecules (AIM) approach is a convenient method used to analyse hydrogen bonding and other interactions in various molecular systems in terms of bond critical points (BCPs). The formation of hydrogen bonds is the result of an interaction between two closed-shell systems, and this is reflected in the properties of the charge distribution, particularly in the electron density (ρ) and the Laplacian of electron density $\nabla^2(\rho)$. The geometrical and topological parameters calculated at BCP are shown in **Table 5**. The molecular graph of both conformers of the title compound showing intramolecular interactions using AIM analysis is shown in **Figure 6**. It can be observed that each hydrogen bond is characterized by the presence of one bond critical point (red spheres) and bond path that connects the N31 of the azomethine group to one H atom belonging to the hydroxyl group, thus confirming the interaction in conformer I, and it was absent in conformer II. The values of ρ at the BCP is a good measure of the strength of the interaction. The largest value (0.03935 a.u.) corresponds to the

intramolecular hydrogen bonding interaction O29-H30···N3, with an interaction energy of -8.67 kcal/mol. Furthermore, the distribution of the BCP reveals the existence of an additional N16-H17···O12 intramolecular hydrogen bond. Each one is characterized by a bond critical point and bond path connecting one hydrogen of the hydrazine group to one oxygen of the nitro group. The values of the Laplacian of electron density at the BCP are positive, which is common in closed-shell interactions. It should be noted that the H···H dispersive interactions play a cooperative role in the structure of conformer II. The interaction energy of O29-H30···H19 contact is calculated to be -3.898 kcal/mol. The relevance of H···H interactions has been analysed in different organic structures reported previously **[40, 41]** and it has been reported that the H···H bonding is a stabilizing interactions in a non-electrostatic nature in molecules and crystals **[42]**.

3.5. Molecular electrostatic potential (MEP)

The molecular electrostatic potential (MEP) surface was investigated in order to explore the substantial electronic structure and properties. The MEP surface for the most stable conformer of 5-Cl-DNPHZ is shown in **Figure 7**. The MEP maps are useful to study the chemical reactivity and the electronic nature of different sites of a molecule. The red and blue colours represent the negative and positive electrostatic potentials, respectively, where blue indicates the strongest attraction and red indicates the strongest repulsion. As can be seen from Fig. 7, the MEP values over the oxygens from the nitro groups are negative with potential values between -18 and -22 kcal/mol, indicating that are the preferred sites of hydrogen bonding interactions. Moreover, a negative electrostatic potential in the region of the hydroxyl oxygen has been also observed. The regions having the most positive electrostatic potentials are over the hydrogen atoms of the azomethine and hydrazine groups. These results indicate that the hydrogen bonding interactions between these groups should be energetically favoured.

4. CONCLUSIONS

A new hydrazone compound 5-chlorosalicylaldehyde-2,4-dinitrophenylhydrazone (5Cl-DNPHZ) has been synthesized and characterized by IR, Raman and UV-Visible spectroscopies. The study is mainly focused on combining both spectroscopic and quantum chemical calculations that could help in a better understanding of solid-state molecular structure from various aspects such as hydrogen bonding , chemical reactivity parameters and the structure-reactivity relationships. The

structural parameters and chemical reactivity of the studied substance and for a related compound previously reported have been computed in gas phase and in solvents with different polarity. The observed frequency values of the IR and Raman spectra were assigned to the appropriate theoretically computed frequency values to validate and correlate both results. The calculated frequency values agree well with the experimental data. The calculated geometrical parameters are in accordance with the experimental ones determined by XRD data for related molecules. The conformational analysis reveal that two possible conformers are possible for the title compound but the most stable conformer is mainly stabilized by intramolecular O29-H30···N31 interaction between the N31 of the azomethine group and the H30 from the hydroxyl group. In addition, the planar conformation in both conformers are also stabilized by intramolecular N16-H···O12 interactions involving the hydrazine N-H and the oxygen from the *ortho* nitro group. AIM calculations suggest that the intramolecular interactions that stabilized the structure of both conformers are *core-shell* interactions in nature. These results are in agreement with NBO calculations indicating that the charge transfer phenomenon, particularly LP O12 → σ* N16-H17 plays an important role in the formation of intramolecular N16-H17···O12 hydrogen bond observed in both conformers, and without these interactions, the stabilization of the title compound is not possible. The total molecular energies obtained by the PCM method decrease with the increasing polarity of the solvent and the stability of the studied compounds increases in going from the gas phase to the solution phase. In parallel, the HOMO-LUMO band gap decreases with the polarity of the solvents indicating that both compounds are more reactive and less stable in polar solvents.

Acknowledgments

The author thank ANPCyT (PICT 2016-0226) and SCAIT (Project D639/2) for financial support.

REFERENCES

[1] N. Ergenç, N.S. Günay, Eur. J. Med. Chem. 33 (1998) 143-148.

[2] X. Deng, N.S. Mani, J. Org. Chem. 73 (2008) 2412.

[3] F. Armbruster, U. Klingebiel, M. Noltemeyer, Z. Naturforsch 61b (2006) 225-236.

[4] S.G. Küçükgüzel, A. Kocatepe, E. De Clercq, F. Sahin, Eur. J. Med. Chem. 41 (2006) 353.

[5] B. Barta Holló, J. Magyari, S. Armaković, G.A. Bogdanović, M.V. Rodić, S.J. Armaković, J. Molnár, G. Spengler, V.M. Leovac, K. Mészáros Szécsényi, New J. Chem. 40 (2016) 5885-5895.

[6] A. A. El-Sherif, A. Fetoh, Y.K. Adulhamed, G.M. Abu El-Reash, Inorg. Chim. Acta 480 (2018) 1-15.

[7] L. Li, Y.Z. Zhang, E. Liu, C. Yang, J.A. Golen, A.L. Rheingold, G. Zhang, J. Mol. Struct. 1110 (2016) 180-184.

[8] R.P. Bakale, G.N. Naik, S.S. Machakanur, C.V. Mangannavar, I.S. Muchchandi, K.B. Gudasi, J. Mol. Struct. 1154 (2018) 92-99.

[9] N. Raman, S. Ravichandran, C. Thangaraja, J. Chem. Sci. 116 (2004) 215-219.

[10] S.A. Abdel Latif, A.A. Mohamed, J. Mol. Struct. 1153 (2018) 248-261.

[11] A. Manimekalai, N. Saradhadevi, A. Thiruvalluvar, Spectrochim. Acta A 77 (2010) 687-695.

[12] R. F. Martinez, M. Ávalos, R. Babiano, P. Cintas, J.L. Jiménez, M.E. Light, J.C. Palacios, Org. Biomol. Chem. 9 (2011) 8268-8275.

[13] X. Shang, J. Yuan, Y. Wang, J. Zhang, X. Xu, J. Mol. Struct. 1010 (2012) 52-58.

[14] S. Rollas, Ş. Güniz Küçükgüzel, Molecules 12 (2007) 1910-1939.

[15] G. Verma, A. Marella, M. Shaquiquzzaman, M. Akhtar, M. Ali, M. Alam, J. Pharm. Bioallied Sci. 6 (2014) 69-80.

[16] M. Mohan, M.P. Gupta, L. Chandra, N.K. Jha, Inorg. Chim. Acta 151 (1988) 61.

[17] M. Jesmin, M.M. Ali, J.A. Khanam, Thai J. Pharm. Sci. 34 (2010) 20–31.

[18] O.G. Idemudia, A.P. Sadimenko, E.C. Hosten, Acta Cryst. E68 (2012) o3380.

[19] O.G. Idemudia, A.P. Sadimenko, A.J. Afolayan, E.C. Hosten, Bioinorg. Chem. Appl. 2015 (2015) 717089.

[20] N.N. Ji, Z.Q. Shi, R.G. Zhao, Z.B. Zheng, Z.F. Li, Bull. Korean Chem. Soc. 31 (2010) 881-886.

[21] H.H. Monfared, O. Pouralimardan, C. Janiak, Z. Naturforsch. 62b (2007) 717-720.

[22] O.G. Idemudia, E.C. Hosten, Crystals 6 (2016) 127.

[23] M.J. Frisch, J.A. Pople, J.S. Binkley, *J. Chem. Phys*. 1984, **80**, 3265. M.J. Frisch, G.W. Trucks, H.B. Schlegel, G.E. Scuseria, M.A. Robb, J.R. Cheeseman, J.A. Montgomery Jr., T. Vreven, K.N. Kudin, J.C. Burant, J.M. Millam, S.S. Iyengar, J. Tomasi, V. Barone, B. Mennucci, M. Cossi, G. Scalmani, N. Rega, G.A. Petersson, H.

Nakatsuji, M. Hada, M. Ehara, K. Toyota, R. Fukuda, J. Hasegawa, M. Ishida, T. Nakajima, Y. Honda, O. Kitao, H. Nakai, M. Klene, X. Li, J.E. Knox, H.P. Hratchian, J.B. Cross, C. Adamo, J. Jaramillo, R. Gomperts, R.E. Stratmann, O. Yazyev, A.J. Austin, R. Cammi, C. Pomelli, J.W. Ochterski, P.Y. Ayala, K. Morokuma, G.A. Voth, P. Salvador, J.J. Dannenberg, V.G. Zakrzewski, S. Dapprich, A.D. Daniels, M.C. Strain, O. Farkas, D.K. Malick, A.D. Rabuck, K. Raghavachari, J.B. Foresman, J.V. Ortiz, Q. Cui, A.G. Baboul, S. Clifford, J. Cioslowski, B.B. Stefanov, G. Liu, A. Liashenko, P. Piskorz, I. Komaromi, R.L. Martin, D.J. Fox, T. Keith, M.A. Al- Laham, C.Y. Peng, A. Nanayakkara, M. Challacombe, P.M.W. Gill, B. Johnson, W. Chen, M.W. Wong, C. González, J.A. Pople, Gaussian 03, revision C.02, GaussianInc., Wallingford, CT, 2004.

[24] A.E. Reed, L.A. Curtiss, F. Weinhold, Chem. Rev. 88 (1988) 899-926.

[25] R.F.W. Bader, Atoms in Molecules: A Quantum Theory, Clarendon Press, Oxford, 1990.

[26] F. Biegler-König, J. Schönbohm, D. Bayles, J. Comput. Chem. 22 (2001) 545.

[27] M. Cossi, N. Rega, G. Scalmani, V. Barone, J. Comput. Chem. 24 (2003) 669.

[28] A.K. Singh, R.K. Singh, J. Mol. Struct. 1089 (2015) 191-205.

[29] M. Bakir, J. Mol. Struct. 1173 (2018) 942-950.

[30] P. Rawat, R.N. Singh, J. Mol. Struct. 1097 (2015) 214-225.

[31] R.K. Singh, A.K. Singh, J. Mol. Struct. 1129 (2017) 128-141.

[32] M.R. Rodríguez, J. Del Plá, O.E. Piro, G.A. Echeverría, G. Espino, R. Pis-Diez, B.S. Parajón-Costa, A.C. González-Baró, J. Mol. Struct. 1165 (2018) 381-390.

[33] Y. Kaya, C. Icsel, V.T. Yilmaz, O. Buyukgungor, J. Mol. Struct. 1095 (2015) 51-60.

[34] J. Coates. Interpretation of Infrared Spectra. A practical approack, Encyclopedia of Analytical Chemistry. Wiley. 2006.

[35] V. Arjunan, S. Mohan, S. Subramanian, B. Thimme Gowda, Spectrochim. Acta A 60 (2004) 1141-1159.

[36] C. Arunagiri, A. Subashini, M Saranya, P. Thomas Muthiak, K. Thanigaimani, I. Abul Razak, Spectrochim. Acta A 135 (2015) 307-316.

[37] M.R. Anoop, P.S. Binil, S. Suma, M.R. Sundarsanakumar, S. Mary, H.T. Varghese, C.Y. Panicker, J. Mol. Struct. 969 (2010) 48-54.

[38] R.M. Silverstein, F.X. Webster, Spectrometric Identification of Organic Compounds, Sixth Ed. Jon Wiley Sons. Inc., New York, 1963.

[39] M. Rocha, A. Di Santo, J.M. Arias, D.M. Gil, A. Ben Altabef, Spectrochim. Acta A 136 (2015) 635-643.

[40] P. Venkatesan, M. Cerón, S Thamotharan, F. Robles, M.J. Percino, CrystEngComm 20 (2018) 2681-2697.

[41] S. Thamontharan, J. Kothandapani, S. Selva Ganesan, N.S. Venkataramanan, S. Madan Kumar, K. Byrappa, J. Percino, F. Robles. J. Chem. Sci. 130 (2018) 20.

[42] C.F. Matta, T.H. Hernandez-Trujillo, J. Fau-Tang, R.F.W. Tang Th Fau-Bader, R.F. Bader, Chem. Eur. J. 9 (2003) 1940-1951.

Table 1: Geometrical parameters (bond lengths, angles and torsional angles) for the two possible conformers of 5Cl-DNPHZ calculated at B3LYP/6-311++G(d,p) approximation. The computed parameters were calculated with experimental values reported in literature.

Parameters	Calculated [B3LYP/6-311++G(d,p)]		Experimental [a]
	CI conformer	CII conformer	
Bond lengths (Å)			
C18-N31	1.293	1.286	1.287
N31-N16	1.360	1.356	1.376
N16-C3	1.360	1.362	1.342
C20-C18	1.448	1.459	1.472
C20-C21	1.408	1.408	1.398
C21-C23	1.381	1.380	1.381
C23-C26	1.398	1.397	1.363
C26-C25	1.386	1.385	1.385
C25-C22	1.397	1.397	1.376
C22-C20	1.417	1.409	1.390
C22-O29	1.347	1.367	1.368
C3-C4	1.429	1.428	1.416
C4-C5	1.393	1.394	1.381
C5-C6	1.376	1.378	1.366
C6-C1	1.400	1.402	1.398
C1-C2	1.374	1.374	1.360
C2-C3	1.418	1.418	1.418
C4-N10	1.460	1.459	1.443
C6-N13	1.468	1.468	1.446
N10-O11	1.219	1.220	1.223
N10-O12	1.243	1.243	1.238
N13-O14	1.225	1.225	1.228
N13-O15	1.226	1.227	1.226
C23-Cl32	1.757	1.758	-
O29-H30···N31	1.821	-	-
N16-H17···O12	1.828	1.841	-
Bond angles (º)			
C20-C18-N31	122.6	122.1	115.2
C18-N31-N16	116.7	116.6	117.2
N31-N16-C3	122.2	121.2	119.4
N16-C3-C2	120.9	120.3	119.9
N16-C3-C4	122.2	122.5	123.5
N10-C4-C5	116.2	116.3	115.9
N10-C4-C3	122.6	122.5	121.9
C5-C6-N13	119.3	119.3	119.0
C1-C6-N13	119.7	119.6	119.9
Torsional angles (º)			
C21-C20-C18-N31	-179.9	-14.23	167.3
C20-C18-N31-N16	179.9	177.2	-178.6
C18-N31-N16-C3	179.9	178.4	-173.6
N31-N16-C3-C4	179.9	179.6	-178.9

N31-N16-C3-C2	-0.004	-0.392	2.500

[a] Taken from Ref. [20]

Table 2: Experimental and calculated frequencies (cm^{-1}) of the most stable conformer (CI) of 5-Cl-DNPHZ and tentative assignment of modes.

Experimental [a]		Calculated [b]		Tentative assignment of modes (PED %) [c]
IR	Raman	Unscaled	Scaled	
3360 br	-	3496	3384	υ OH (99)
3287 w	3289	3431	3321	υ NH (99)
3102 vvw	-	3189	3087	υ CH-R1 (98)
3079 vvw	-	3067	2968	υ C18-H (100)
1618 s	1615	1656	1603	υ CC-R1 (52); δ COH (10)
1607 sh	1603	1653	1599	υ CC-R2 (48); δ CCH-R1 (10)
1582 m	1580	1647	1594	υ C18=N31 (44)
-	1560	1628	1576	υ CC-R2 (34); δ NNH (11)
1543 vw	-	1601	1550	υ_a NO_2 (52); δ NNH (28)
-	1529	1598	1547	υ CC-R1 (44); υ CN (12); δ COH (12)
1513 s	1511	1564	1514	υ CC-R2 (76)
1479 w	1476	1506	1458	δ CCH-R1 (47); δ CCC-R1 (23)
-	1447	1482	1434	δ CCH-R2 (25)
1417 w	1418	1465	1418	δ COH (31)
1392 vw	1391	1452	1405	υ CC-R2 (40); δ CCH (10); υ_a NO_2 (10)
-	1364	1421	1375	υ CC-R1 (26) ; δ CCH-R1 (14); δ COH (13)
1336 vs	1336	1353	1310	υ_s NO_2 (39); δ CCH-R2 (12)
1311 w	1305	1343	1300	υ CC-R1 (52); υ CC-R2 (11)
-	1296 sh	1338	1295	υ_s NO_2 (13); δ CCH-R2 (10)
1278 w	1274	1300	1258	υ C-O (36)
1264 w	1263	1286	1245	δ CCH-R2 (32); υ_s NO_2 (22)
1224 vw	1228	1258	1218	δ CCH-R1 (41)
1209 vvw	1206	1242	1202	δ CCH-R2 (26); δ NNH (27)
1188 w	1186	1221	1182	υ CC-R1 (48); δ CCH-R1 (11)
1149 m	1147	1169	1131	υ NN (25); δ CCH-R2 (20)
1134 w	1133	1153	1116	υ CC-R2 (24); δ CCH-R2 (14); δ CCH-R1 (11)
1103 w	1101	1147	1110	δ CCH-R1 (35); υ CC-R2 (13)
-	1088	1127	1091	υ NN (31); δ CCC-R2 (15)
1060 vw	1058	1106	1070	υ CC-R1 (51); δ CCH-R1 (25)
962 vvw	960	997	965	γ CH-R2 (79)
938 vvw	950	975	944	γ C18-H (79)
-	935	964	933	γ CH-R1 (82)
925 w	923	954	923	γ CH-R2 (86)
917 w	-	952	921	δ CCC-R1 (41)
883 vvw	-	936	906	υ C-NO_2 (29); δ CCN (11)
834 w	845	867	839	γ OH (88)
821 w	830	851	824	δ NO_2 (58)
743 w	-	794	769	δ CCC-R1 (17); δ CCC-R2 (12)
729 w	724	741	717	δ CCN (23)
704 vw	703	731	708	γ NO_2 (78)
681 vvw	-	713	690	γ NO_2 (79)
664 vvw	661	678	656	δ CCC-R2 (61)
657 vvw	-	677	655	γ NH (52); γ CCC-R2 (14)
644 vvw	640	668	647	γ CCC-R2 (42); γ NH (36)
624 vvw	624	642	621	δ CCC-R1 (91)
605 vvw	-	634	614	δ CCC-R2 (35)

590 vvw	591	573	555	γ CCNN (50); γ CCCC-R2 (22)
533 vvw	529	537	520	δ CON (58)
488 vvw	490	500	484	γ CCCN-R2 (66)
475 vvw	472	478	463	δ CCC (27); δ CCN (11)
468 vvw	464	474	459	γ CCCC-R1 (55); γ CH-R1 (10)
411 vw	413	425	411	γ CCCC-R2 (63)
-	378	384	372	δ CCC-R1 (41); υ C-Cl (18)
-	359	365	353	δ CCC-R1 (40); υ C-Cl (13)
-	321	326	316	δ CC-NO_2 (65)
-	288	304	294	γ CCNN (64)
-	249	277	268	δ CC-Cl (53)
-	180	183	177	δ CCN (52)
-	166	158	153	γ NCCC (55)
-	151	155	150	δ CCN (32); υ NN (11)
-	126	127	123	δ CCC (38)
-	107	119	115	τ CCNN (53)
-	72	80	77	τ CCCN (72)
-	55	58	56	τ CCNO (85)

[a] vs: very strong, s: strong, m: medium, w: weak, vw: very weak, vvw: extremely weak, sh: shoulder.

[b] Calculated frequencies at B3LYP/6-311++G(d,p) level. Scale factor: 0.9679

[c] υ: stretching, δ: bending, γ: out-of-plane bending, τ: torsional modes. R1: C20-C21-C23-C26-C25-C22 and R2: C1-C6 phenyl rings.

Table 3: Experimental and calculated electronic transitions for 5-Cl-DNPHZ along with their assignments.

Wavelength (nm)		Oscillator strength (*f*)	Assignment
Experimental [a]	Calculated [b]		
-	463	0.1989	HOMO → LUMO (100 %)
506	417	0.4905	HOMO → LUMO+1 (100 %)
478	349	0.3278	HOMO-1 → LUMO (100 %)
386	264	0.2635	HOMO-3 → LUMO (87 %)
			HOMO-2 → LUMO+1 (13 %)

[a] Experimental spectrum measured in DMF.
[b] Calculated UV-Vis at B3LYP/6-311++G(d,p) level taking into account the implicitly of the solvent (DMF).

Table 4: Stabilization energies $E^{(2)}$ of interacting natural bond orbitals of 5-Cl-DNPHZ.

Donor (i)[a]	Acceptor (j)	Stabilization energy, $E^{(2)}$ (kcal/mol)	
		Conformer I	***Conformer II***
LP O11	σ* C4-N10	18.35	18.26
LP O11	σ* N10-O12	22.66	22.65
LP O12	σ* C4-N10	13.40	13.43
LP O12	σ* N10-O11	19.73	19.78
LP O12	σ* N16-H17	17.32	16.53
LP O12	π* N10-O11	133.3	133.3
LP N16	π* C3-C4	54.82	54.44
LP N16	π* C18-N31	27.37	29.35
LP O29	π* C22-C25	34.31	25.88
LP Cl32	π* C23-C26	17.75	18.14
π C22-C25	π* C23-C26	26.83	24.88
π C23-C26	π* C20-C21	24.51	24.27
π C23-C26	π* C22-C25	16.31	17.51
π C20-C21	π* C18-N31	26.51	19.00
π C1-C2	π* C3-C4	23.45	23.46
π C3-C4	π* C5-C6	25.97	25.77
π C3-C4	π* N10-O11	32.31	32.57
π C5-C6	π* C1-C2	22.22	21.56
π C5-C6	π* N13-O14	23.95	23.93

[a] LP denotes the lone pair on the specified atom.

Table 5: Topological parameters for bonds of interacting atoms: electron density (ρ), Laplacian of electron density ($\nabla^2\rho$), electron kinetic energy density (G), total electron energy density (H), electron potential energy density (V) at the bond critical point (BCP) and estimated interaction energy (E_{HA}) in kcal/mol for 5Cl-DNPHZ.

Interactions	ρ (a.u.)	$\nabla^2\rho$ (a.u.)	G (a.u.)	H (a.u.)	V (a.u.)	E_{HA} (kcal/mol)
Conformer I						
O29-H30···N31	0.03935	0.1105	0.03091	0.00329	-0.02762	-8.670
N16-H17···O12	0.03680	0.1370	0.03319	-0.00108	-0.03427	-10.75
Conformer II						
O29-H30···H19	0.01285	0.0497	0.01044	-0.00198	-0.01243	-3.898
N16-H17···O12	0.03588	0.1346	0.03231	-0.00134	-0.03365	-10.56

Figures

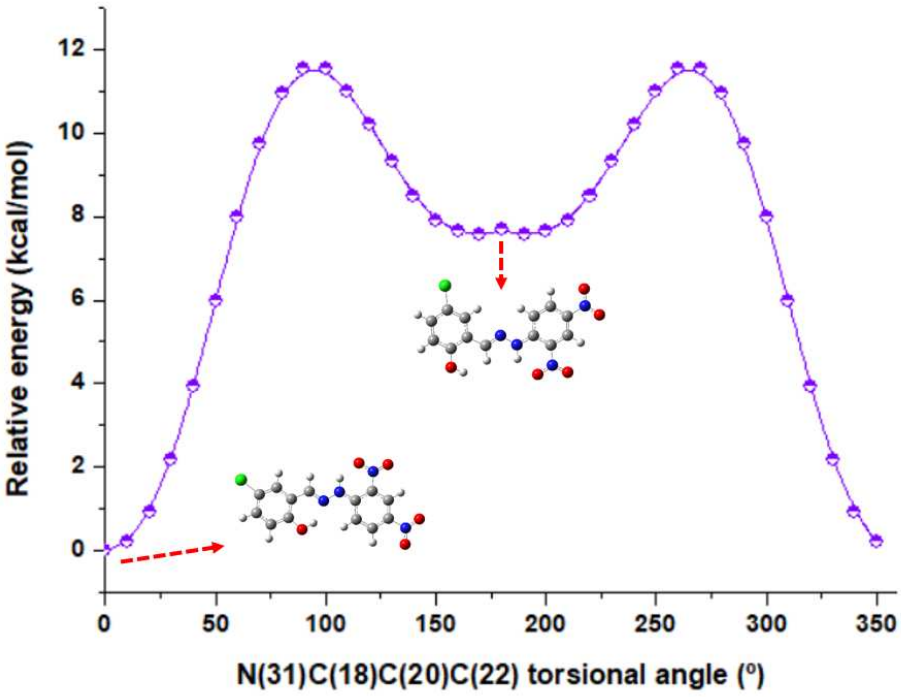

Figure 1: Potential energy curve around the C18-C20 bond at B3LYP/6-311++G(d,p) level of theory.

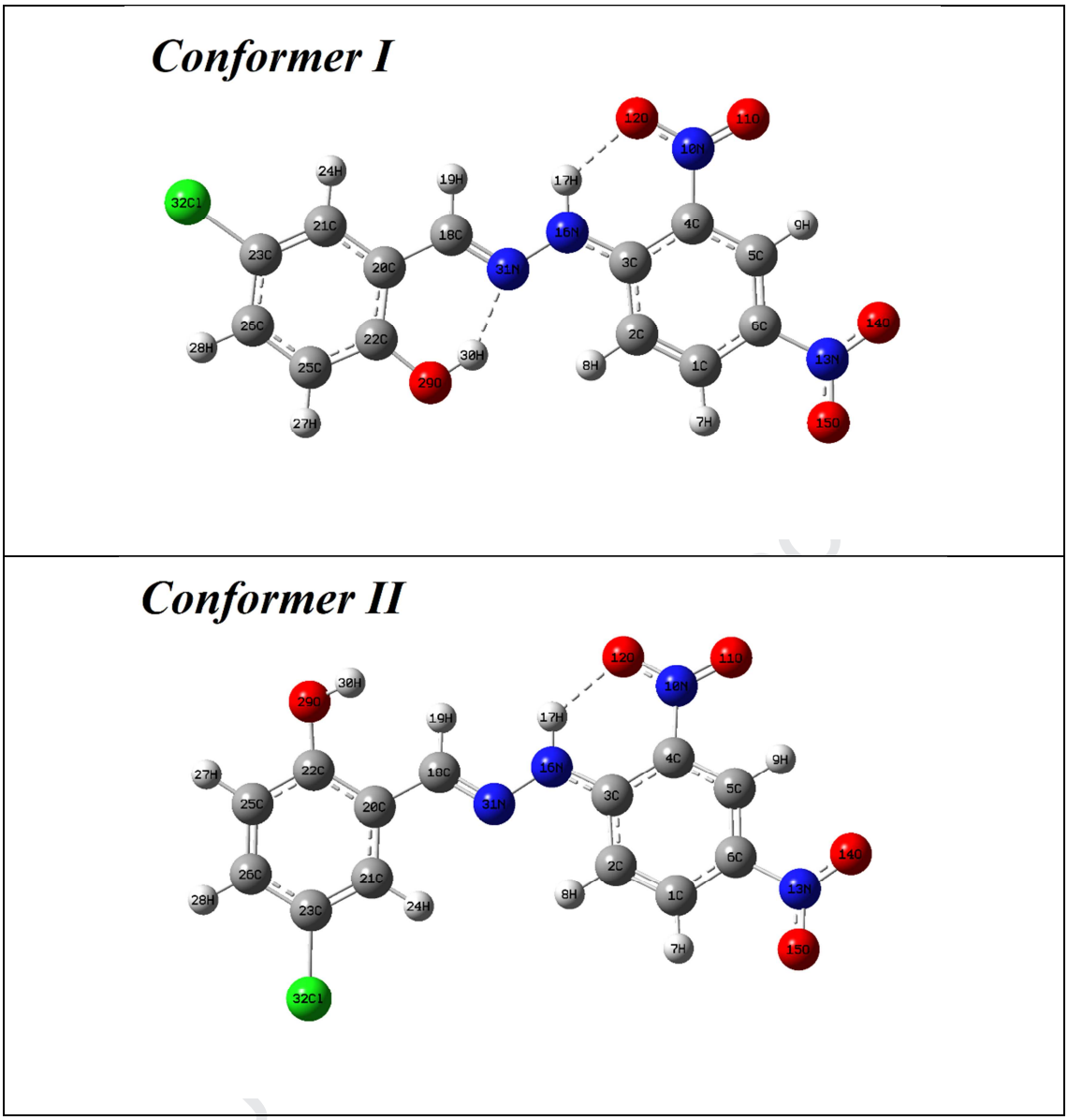

Figure 2. Optimized molecular structures for both possible conformers of 5Cl-DNPHZ.

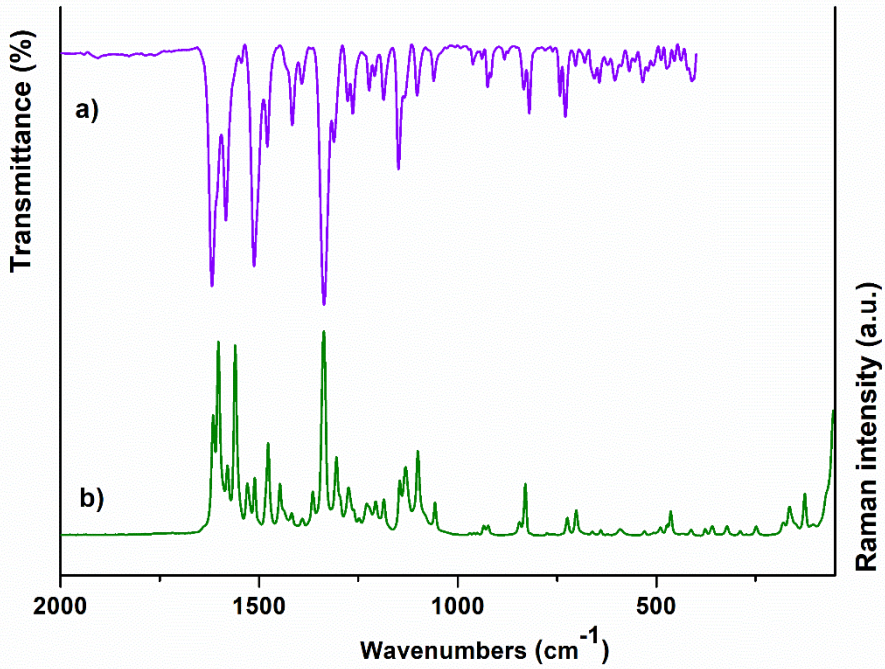

Figure 3: a) FTIR spectra of 5-Cl-DNPHZ in solid state measured at room temperature; **b)** Raman spectrum of 5-Cl-DNPHZ in solid state measured at room temperature.

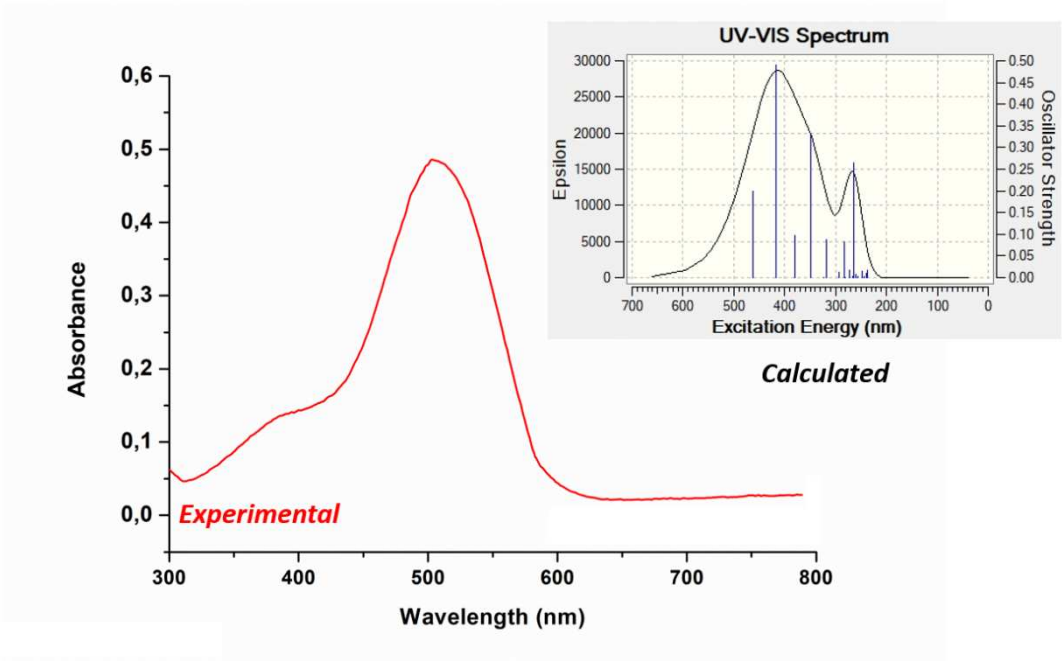

Figure 4: Experimental UV-Vis spectrum of 5-Cl-DNPHZ measured in DMF. Inset: Simulated UV-Vis spectrum computed at B3LYP/6-311++G(d,p) approximation.

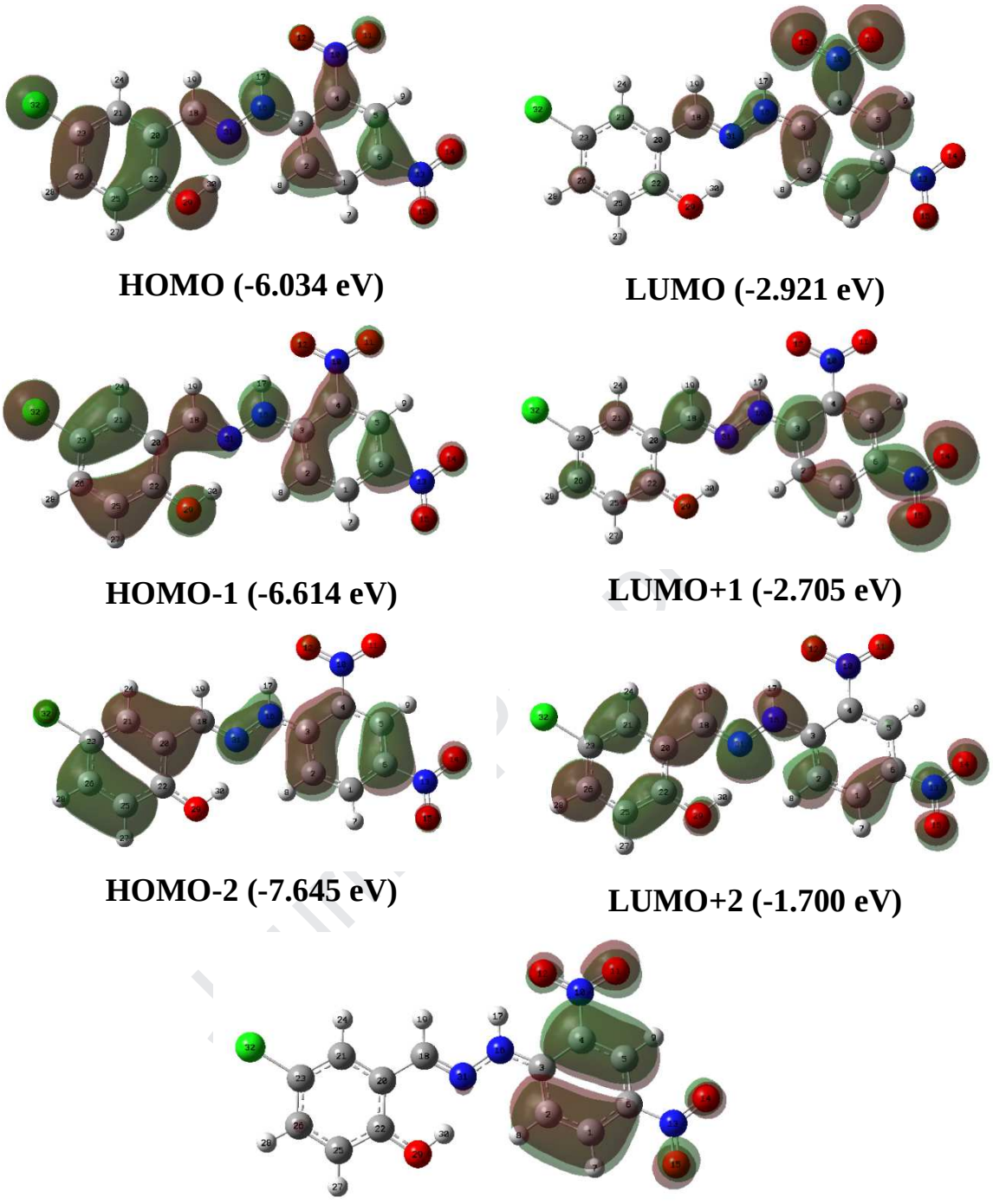

Figure 5: Frontier molecular orbitals for the main electronic transitions for 5-Cl-DNPHZ.

Conformer I

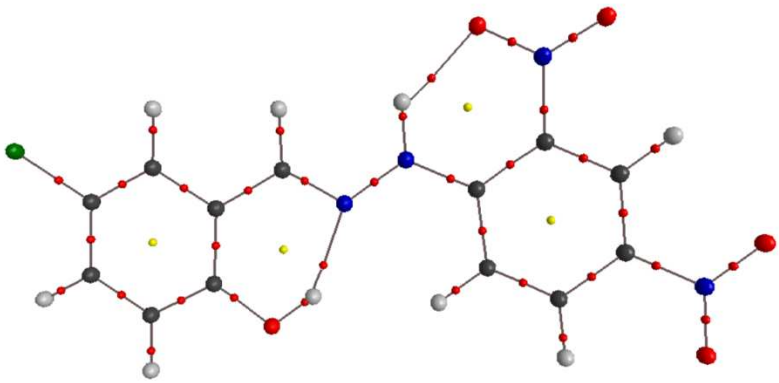

Conformer II

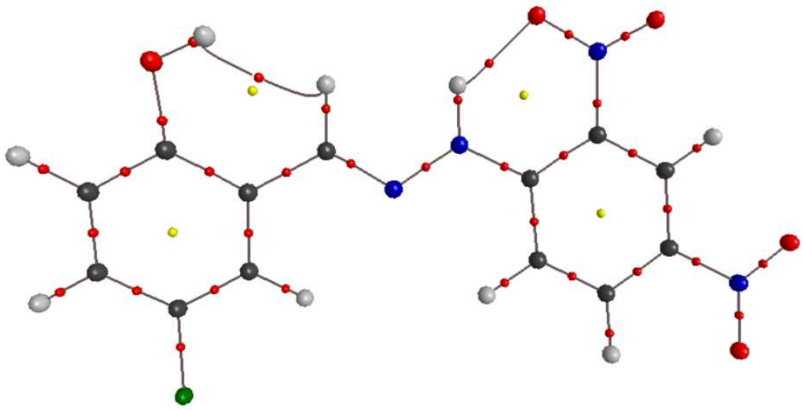

Figure 6: Distribution of bonds and ring critical points (red and yellow spheres, respectively) and bond paths in both conformations of 5-Cl-DNPHZ.

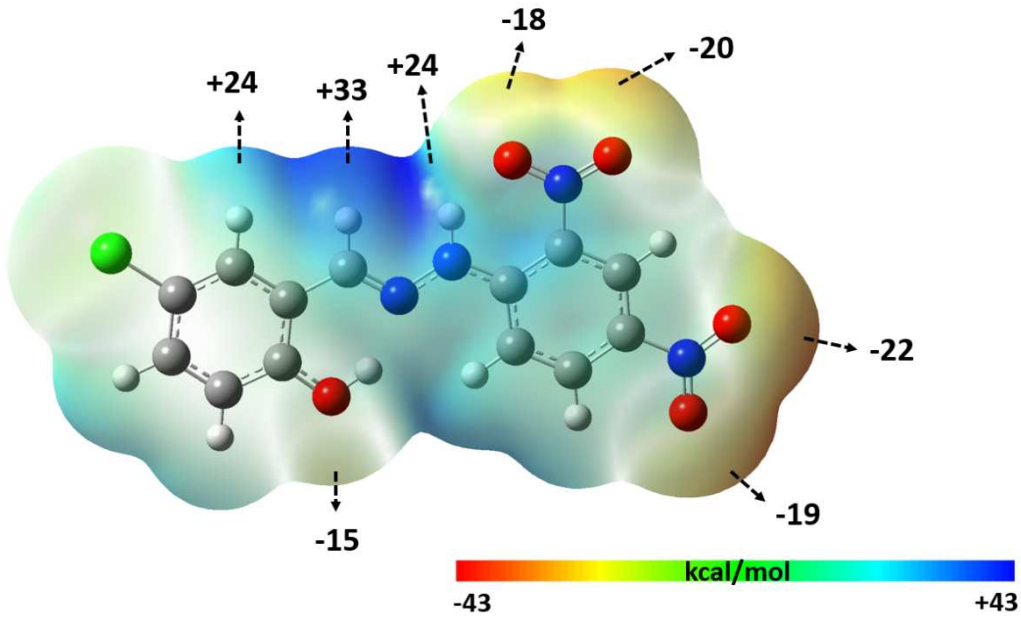

Figure 7: Molecular electrostatic potential (MEP) surface for the most stable conformer of 5-Cl-DNPHZ. MEP values at selected points are given in kcal/mol

Highlights:

- The new hydrazone derivative has been synthesized and characterized.
- The molecular structure was determined by DFT calculations.
- The experimental and computed vibrational frequencies show a good agreement.
- The intramolecular interactions were studied by means NBO and AIM analysis.

Author contribution statement

I have performed the synthesis, the experimental measurements and the theoretical study reported in this work. I have also written the whole manuscript.